

Ingrowing Kardar-Parisi-Zhang interfaces – experimental and numerical investigations

Yohsuke T. Fukai^{1,2,*} and Kazumasa A. Takeuchi^{2,†}

¹*Department of Physics, the University of Tokyo*

²*Department of Physics, Tokyo Institute of Technology*

(Dated: May 19, 2022)

We investigate fluctuation properties of the $(1+1)$ -dimensional Kardar-Parisi-Zhang (KPZ) interfaces growing inward from ring-shaped initial conditions experimentally and numerically, using growth of a turbulent state in liquid-crystal electroconvection and an off-lattice Eden model, respectively. It is shown that statistical properties agree with those of the KPZ subclass for flat interfaces, specifically the Tracy-Widom distribution for the Gaussian orthogonal ensemble and the Airy_1 spatial correlation function, in spite of the non-zero curvature of the initial conditions. At a characteristic time determined by the initial curvature, the interfaces depart from the KPZ roughening regime. We give an explanation to this deviation in terms of the correlation length and the circumference. Our results indicate that the sign of the initial curvature has a crucial role to determine the asymptotic distribution and correlation functions.

The concept of universality classes, which was originally introduced in the field of critical phenomena, is now extending the applicability to scale invariant phenomena in out-of-equilibrium systems. A prototypical example is interface growth phenomena, in which scale-invariant fluctuations often appear spontaneously without fine tuning of the system parameters [1]. In particular, the $(d+1)$ -dimensional Kardar-Parisi-Zhang (KPZ) equation [2] describes generic situations without conservation laws, which reads, for interface height $h(x, t)$ at position $x \in \mathbb{R}^d$ and time $t \in \mathbb{R}$,

$$\frac{\partial}{\partial t} h(x, t) = \nu \nabla^2 h(x, t) + \frac{\lambda}{2} (\nabla h(x, t))^2 + \eta(x, t) \quad (1)$$

where η is a Gaussian noise satisfying $\langle \eta(x, t) \rangle = 0$ and $\langle \eta(x, t) \eta(x', t') \rangle = D \delta(x - x') \delta(t - t')$. For the KPZ equation, the fluctuation amplitude $\delta h := h(x, t) - \langle h(x, t) \rangle$ and the correlation length $\xi(t)$ follow the scaling laws, $\delta h \sim t^\beta$ and $\xi(t) \sim t^{1/z}$ respectively, which determine the universal exponents β and z . In particular, for $1+1$ dimension, these exponents are $\beta = 1/3$ and $z = 3/2$ [1–3]. The same exponents as the KPZ equation have been found not only in theoretical models [4] but also in various phenomena such as bacterial colony growth [5], paper combustion [6], liquid-crystal electroconvection [7–9], eukaryotic cell colony growth [10], particle deposition in coffee ring effect [11] and chemical reaction front [12] forming the KPZ universality class [4, 13].

The height of interfaces in the $(1+1)$ -dimensional KPZ universality class is expected to follow

$$h(x, t) \simeq v_\infty t + (\Gamma t)^{\frac{1}{3}} \chi(x', t) \quad (2)$$

$$x' := x/\xi(t), \quad \xi(t) := \frac{2}{A} (\Gamma t)^{\frac{2}{3}} \quad (3)$$

for large t , as long as the system size is much larger than the correlation length (roughening regime), where $v_\infty, A > 0, \Gamma \in \mathbb{R}$ are system-dependent non-universal parameters. For isotropic interfaces, $\Gamma > 0$ and $A =$

$\sqrt{2\Gamma/v_\infty}$ can be shown [9]. The stochastic variable $\chi(x', t)$ represents the rescaled height and $\xi(t)$ the correlation length.

From the 2000s, theoretical studies on the $(1+1)$ -dimensional KPZ class have revealed exact statistical properties of $\chi(x', t)$ in $t \rightarrow \infty$ for infinite-size systems, such as the one-point distribution function and two-point spatial correlation function $\text{Cov}[\chi(x' + \zeta, t), \chi(x', t)]$, which were moreover found to be geometry dependent [4]. For example, curved (e.g. droplet-shaped) interfaces and flat interfaces show different one-point distribution functions, specifically, the Tracy-Widom distribution for the Gaussian unitary/orthogonal ensemble (GUE/GOE), respectively (denoted by χ_2/χ_1 here [14]) [15–19], which are known as the largest-eigenvalue distribution of random matrices [20]. Similarly, the spatial correlation for the curved and flat interfaces is given by the Airy_2 and Airy_1 correlation function, respectively [17, 21].

This geometry dependence turned out to be relevant in a real experimental system as well, as shown for the liquid-crystal (LC) electroconvection [7–9]. These experiments investigated the growth of spatiotemporal chaotic state called the dynamic scattering mode (DSM) 2, which contains high density of topological defects, in another spatiotemporal chaotic state, DSM1. The initial cluster of DSM2 was nucleated by ultraviolet (UV) laser light, focused on a point or a line to generate a circular or flat interface, respectively. It was shown that the circular and flat interfaces show statistical properties in agreement with those of the curved-interface models and flat-interface models, respectively. With those theoretical and experimental results, it is now established that the circular and flat *universality subclasses* exist, which are characterized by the same exponents yet different universal statistical properties.

However, in contrast to the detailed knowledge on each of the universality subclasses, relevant parameters that determine the subclass to arise still remain unclear. In this Letter, we shed light on this problem by clarifying

how the *sign* of the initial curvature affects the universality subclass of the interfaces. With this aim, we investigate KPZ interfaces growing inward from ring-shaped initial conditions experimentally and numerically.

As the experimental system, we investigated the DSM2 growth in LC electroconvection with a similar setup as the previous experiments [7–9], where we can achieve high statistical accuracy and control the initial condition relatively easily by controlling the beam profile of the UV laser. We prepared a liquid-crystal cell composed of two glass plates with transparent electrodes, separated by spacers of $12\ \mu\text{m}$ thickness. At the center of the cell, liquid crystal *N*-(4-Methoxybenzylidene)-4-butylaniline doped with 0.01 wt % of tetra-*n*-butylammonium bromide was injected in a $1.5\ \text{cm} \times 1.5\ \text{cm}$ area enclosed by the spacers. The electrodes were coated by *N,N*-dimethyl-*N*-octadecyl-3-aminopropyltrimethoxysilyl chloride to obtain the homeotropic alignment. The cutoff frequency separating the conductive and dielectric regimes [22] was $1.77(5) \times 10^3\ \text{Hz}$. We observed an area of about $4\ \text{mm} \times 3\ \text{mm}$ at the center. The cell was attached to a temperature controller, in which the temperature was fixed to $25\ ^\circ\text{C}$. We applied 520 Hz 26 V AC voltage to the liquid-crystal cell. Temperature and voltage fluctuations were about $\pm 0.001\ ^\circ\text{C}$ and $\pm 0.02\ \text{V}$, respectively, during the experiment.

In order to realize a ring-shaped DSM2 initial cluster in LC electroconvection, we constructed an optical setup (Fig. 1(a)) using a spatial light modulator (SLM, Hamamatsu Photonics, LCOS-SLM X10468-05) with which we can control the phase profile of laser light at the resolution of 792×600 pixels in $16\ \text{mm} \times 12\ \text{mm}$. We tuned the phase profile output to the SLM by iterative Fourier transform algorithm [23] so that the Fourier-transformed laser profile has a ring-shaped amplitude profile [24]. The LC cell was illuminated by a light emitting diode (LED), and the transmitted light was recorded by a CCD camera. Example images of growing DSM2 are shown in Fig.1(b). To define the height $h(x, t)$, we first determined the center of the polar coordinate, using the ensemble average of the images taken at the first frame used in the analysis. Then $h(x, t)$ was defined as the displacement from the initial circle in the radial direction and x is measured along a circle, whose radius is equal to the mean radius of the interfaces at time t (Fig.1(b)). The overhangs were averaged out.

We observed nearly 1500 samples (see Table I) with ring initial conditions of different radius, $R_0 = 1526\ \mu\text{m}$ and $1145\ \mu\text{m}$. Errors in R_0 were in the order of $10\ \mu\text{m}$. We also observed 1374 samples of the flat interfaces with the line initial condition, whose length is about twice as long as the width of the observation area.

Figure 2(a) shows the skewness and kurtosis of the height distribution function [25]. The values for the flat interfaces agree with those of χ_1 within the statistical er-

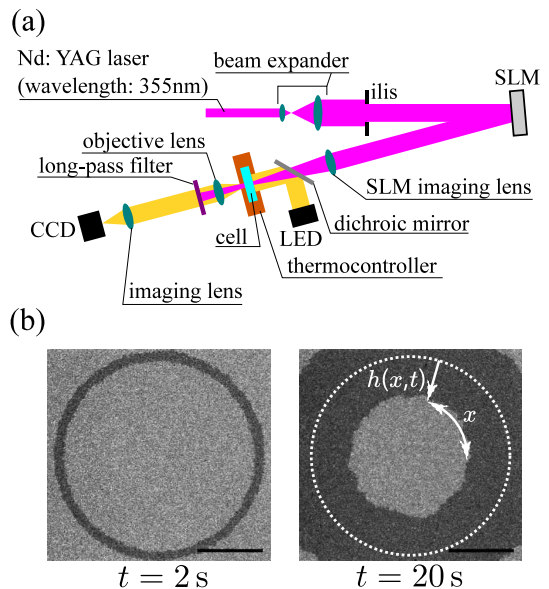


FIG. 1. (color online) (a) Schematic view of the optical setup. SLM: spatial light modulator, CCD: charge-coupled device camera, LED: light-emitting diode. The whole optical setup is placed in an isothermal chamber as in Ref. [9]. (b) Images of the DSM2 growth. The times below the images are the elapsed time after shooting the laser. The scale bar is 1 mm. The dotted line in the right figure denotes the initial condition estimated from the averaged images taken at the first frame used in the analysis.

ror, as expected. For the ingrowing interfaces, the skewness and kurtosis agree with those of the flat interfaces for $t \lesssim 10\ \text{s}$ and differ from the values of χ_2 . At $t \gtrsim 10\ \text{s}$, there seems to be a deviation from the χ_1 values, despite relatively large statistical errors.

We estimated the non-universal parameters v_∞ and Γ using the relationship $\langle \partial_t h \rangle \simeq v_\infty + \text{const.} \times t^{-2/3}$ and $\langle h^3 \rangle_c \simeq \Gamma t \langle \chi^3 \rangle_c$, respectively, expected from Eq. (2). Here, $\langle \dots \rangle_c$ denotes the n -th cumulant and, based on the results of the skewness and kurtosis, we assumed $\langle \chi^3 \rangle_c = \langle \chi_1^3 \rangle_c$. The estimated values are summarized in Table I. Using the estimated Γ , we obtained the cumulants of the rescaled height $q(x', t) := (\Gamma t)^{-1/3} (h(x', t) - v_\infty t)$ with $x' := x/\xi(t)$, for $1 \leq n \leq 4$. The experimental accuracy was not sufficient to draw a conclusion about the 1st cumulant, which was largely dependent on the estimation of R_0 and v_∞ , and the 4th cumulant due to large statistical errors. However, for

TABLE I. Conditions and the non-universal parameters for the LC electroconvection experiment.

initial condition	sample number	v_∞ ($\mu\text{m/s}$)	Γ ($\mu\text{m}^3/\text{s}$)
flat	1374	30.30(7)	$1.84(11) \times 10^3$
$R_0 = 1526\ \mu\text{m}$ ring	1489	30.89(7)	$1.94(6) \times 10^3$
$R_0 = 1145\ \mu\text{m}$ ring	1484	31.00(4)	$1.88(8) \times 10^3$

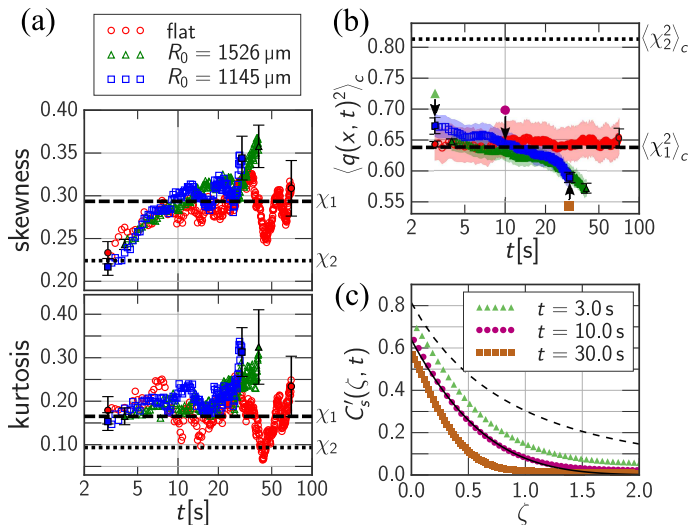


FIG. 2. (color online) The experimental results for the DSM2 growth. (a) The skewness and kurtosis of the height distribution function. The errorbars at the first and last points show the statistical errors. The values of χ_1 and χ_2 are shown by the broken and dotted lines, respectively. (b) The 2nd cumulants of the rescaled height distribution function. The markers are the same as those for (a). The shaded area represents the error from the estimation of Γ and the errorbars at the first and last points show the statistical errors. The values of χ_1 and χ_2 are shown by broken and dotted lines, respectively. The values of time used in (c) are indicated by arrows and symbols used in (c). (c) The rescaled two-point spatial correlation function $C'_s(\zeta, t)$ with rescaled length ζ for the $R_0 = 1145 \mu\text{m}$ ingrowing interfaces. The solid and broken lines represent the Airy₁ and Airy₂ correlation function, respectively.

the ingrowing interfaces, we found that the 2nd cumulant is close to $\langle \chi_1^2 \rangle_c$ for $t \lesssim 10\text{ s}$ and clearly different from $\langle \chi_2^2 \rangle_c$, being consistent with the results of the skewness and kurtosis. For $t \gtrsim 10\text{ s}$, the 2nd cumulant deviates from $\langle \chi_1^2 \rangle_c$ (Fig.2(b)); we will discuss this behavior later. The rescaled two-point spatial correlation function $C'_s(\zeta, t) := \text{Cov}[q(x' + \zeta, t), q(x', t)]$ agreed with the Airy₁ correlation function while the 2nd cumulant is close to the χ_1 value, which is consistent with the flat subclass behavior (Fig.2(c)).

To better understand the experimental results and check the universality, we numerically investigated growth from ring-shaped initial conditions in an off-lattice Eden model [26], which is an isotropic model in the KPZ universality class. This model consists of a cluster of circular-shaped cells, which are added one by one stochastically according to the procedures described in Ref. [26]. The interface shape is determined by a loop formed by the cells wrapping the cluster (for details, see [26]). We simulated interfaces growing inward from a ring of N circularly arranged cells, with $N = 8000, 16000, 32000, 100000$. The numbers of the

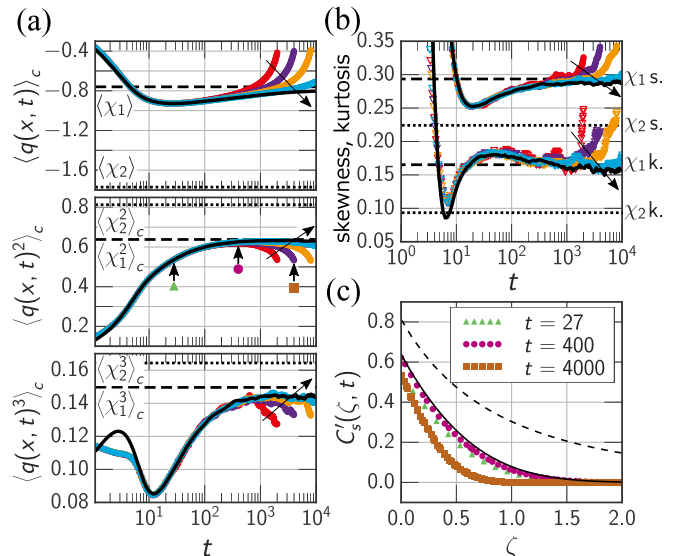


FIG. 3. (color online) The numerical results for the off-lattice Eden model. (a) The cumulants of the rescaled height distribution function for the ingrowing interfaces with $N = 8000, 16000, 32000, 100000$ (colored thick lines) and flat interfaces (black thin lines), in the order of indicated by arrows. The values of χ_1 and χ_2 are shown by broken and dotted lines, respectively. The values of time used in (c) are indicated in the middle plot by arrows and symbols used in (c). (b) The skewness (filled circular markers) and kurtosis (open triangle markers) of the height distribution function. The values of N are the same as those for (a), and indicated likewise. The values of χ_1 and χ_2 are also shown by broken and dotted lines, respectively, where s.=skewness, k.=kurtosis. (c) The rescaled two-point spatial correlation function $C'_s(\zeta, t)$ with rescaled length ζ for the $N = 16000$ ingrowing interfaces. The solid and broken lines represent the Airy₁ and Airy₂ correlation function, respectively.

samples are 2400, 3200, 3200, 1600, respectively. The initial radius R_0 is defined as $R_0 := N/2\pi$. We also simulated flat interfaces from the line initial condition of length 25000 with 3200 samples. We used the values of the non-universal parameters v_∞ and Γ obtained in Ref. [27], while using the values in Ref. [26] did not change the conclusion.

The 1st to 3rd cumulants for the Eden model are shown in Fig.3(a). The cumulants of the ingrowing interfaces approach those of χ_1 in a way similar to the flat interfaces, and deviate from the χ_1 values at a characteristic time, which becomes longer with larger N (i.e. smaller initial curvature). Accordingly, the skewness and kurtosis approach to those of χ_1 and then deviate at the characteristic time (Fig.3(b)). When the cumulants are close to the χ_1 value, the correlation function was also close to the Airy₁ correlation function (Fig.3(c)), as excepted for the flat subclass.

The results for the LC electroconvection and the Eden model agree in the following two points: (1) The cumulants for the ingrowing interfaces approach the χ_1 values

similarly to the flat interfaces, and then deviate at some characteristic times. These values are clearly different from those of χ_2 (Fig.2(a), (b), Fig.3(a), (b)). (2) The correlation functions for the ingrowing interfaces agree with the Airy_1 correlation function while the cumulants are close to the χ_1 values (Fig.2(c), Fig.3(c)).

In Fig.4, we plotted the experimental and numerical data of the cumulants as functions of the rescaled time $\tau := t/t_c = v_\infty t/R_0$, where $t_c := R_0/v_\infty$ indicates an approximate time of the collapse. The numerical data then overlap in the long-time regime $t \approx t_c$, indicating scaling functions that describe the collapse of the ingrowing interfaces. The experimental data also overlap on the same functions within the error, implying universality of the scaling functions. In the short-time regime $t \ll t_c$, the cumulants are expected to stay at the values of χ_1 asymptotically, i.e., in the limit $R_0, t \rightarrow \infty$ with fixed $\tau \ll 1$, since the flat case corresponds to $R_0 \rightarrow \infty$, hence $\tau \rightarrow 0$.

For flat interfaces in a finite-size system, the cumulants are known to deviate from the χ_1 values when the system size is in the same order as the correlation length [28, 29]. This led us to interpret t_c as a time scale at which the system size (namely the circumference) $L(t)$ becomes comparable to the correlation length $\xi(t)$. Because $L(t) \simeq 2\pi(R_0 - v_\infty t)$ and $\xi(t) = \frac{2}{A}(\Gamma t)^{\frac{2}{3}}$, the condition $L(t_c) \approx \xi(t_c)$ gives $t_c \approx R_0/v_\infty$ for $R_0, t \rightarrow \infty$, which is exactly our definition of the characteristic time.

In summary, we investigated the fluctuation properties of KPZ interfaces growing inward from ring-shaped initial conditions, using the DSM2 growth in the LC electroconvection and the off-lattice Eden model. In the short-time regime ($t \ll t_c = R_0/v_\infty$), the observed cumulants of the rescaled height distribution are close to those of the GOE Tracy-Widom distribution, χ_1 , characteristic of the flat subclass. They are significantly different from those of χ_2 for the circular subclass, in spite of the non-zero curvature of the initial interfaces. In this regime, the rescaled two-point spatial correlation function is also close to the Airy_1 correlation function for the flat subclass. Close to the characteristic time $t \approx t_c$, the interfaces depart from the roughening regime. Introducing the rescaled time $\tau = t/t_c$, we found scaling functions of the cumulants that characterize this long-time regime. The agreement in the experimental and numerical data suggests that these scaling functions are universal. This behavior is argued to occur when the correlation length becomes longer than the system size.

Our result indicates that it is not only the existence of the initial curvature that determines the universality subclass, but the sign of the initial curvature is also crucial. Why do the ingrowing interfaces show the flat subclass behavior instead of the circular subclass? Although the reason remains unclear, it may be useful to note that most examples of interfaces in the circular KPZ subclass are outgrowing, in the sense that the effective system size

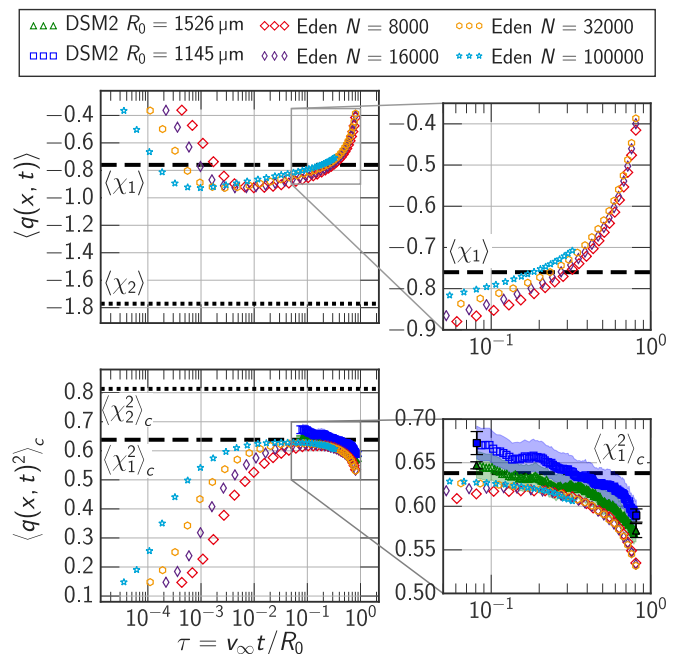


FIG. 4. (color online) The 1st and 2nd cumulants of $q(x', t)$ plotted as functions of the rescaled time $\tau = v_\infty t/R_0$ for the DSM2 growth (the triangle and square markers with errorbars and shaded areas, defined in the same way as Fig.2(b)) and Eden model (the other markers). Only the data for ingrowing interfaces are shown. The experimental data are plotted only for the 2nd cumulant.

increases with time [7, 15, 16, 19, 30]. In contrast, the ingrowing case we study here has the decreasing system size. It is therefore interesting to investigate whether other systems with decreasing system size also show the flat subclass behavior. One may also need to reinterpret the result of the coffee-ring experiment [11], where they investigated interfaces growing inward from the curved edge of a droplet and reported the skewness and kurtosis for the circular subclass. We hope that our results trigger theoretical and mathematical studies as well, and eventually the relevant parameters controlling the split of the KPZ subclasses will be clarified.

We acknowledge discussions on the experimental and numerical methods with M. Sano, on theoretical aspects with T. Sasamoto, H. Spohn, P. Le Doussal, H. Chaté, on interpretations of the results with R. A. L. Almeida. We thank F. Bornemann for the theoretical curve of the Airy_1 and Airy_2 correlation functions [31]. We thank M. Kuroda for technical supports. This work is supported in part by KAKENHI from JSPS (No. JP25103004) and the National Science Foundation under Grant No. NSF PHY11-25915.

* ysk@yfukai.net

† kat@kaztake.org

- [1] A.-L. Barabási and H. E. Stanley, *Fractal Concepts in Surface Growth* (Cambridge University Press, New York, NY, USA, 1995).
- [2] M. Kardar, G. Parisi, and Y.-C. Zhang, *Phys. Rev. Lett.* **56**, 889 (1986).
- [3] D. Forster, D. R. Nelson, and M. J. Stephen, *Phys. Rev. A* **16**, 732 (1977).
- [4] For recent reviews on theoretical studies, see T. Kriecherbauer and J. Krug, *J. Phys. A: Math. Th.* **43**, 403001 (2010); I. Corwin, *Rand. Mat.: Th. Appl.* **01**, 1130001 (2012); J. Quastel and H. Spohn, *J. Stat. Phys.* **160**, 965 (2015); T. Sasamoto, *Prog. Th. Exp. Phys.* **2016**, 022A01 (2016) etc.
- [5] J.-i. Wakita, H. Itoh, T. Matsuyama, and M. Matsushita, *J. Phys. Soc. Jpn.* **66**, 67 (1997).
- [6] J. Maunuksela, M. Myllys, O.-P. Kähkönen, J. Timonen, N. Provatas, M. J. Alava, and T. Ala-Nissila, *Phys. Rev. Lett.* **79**, 1515 (1997); M. Myllys, J. Maunuksela, M. Alava, T. Ala-Nissila, J. Merikoski, and J. Timonen, *Phys. Rev. E* **64**, 036101 (2001).
- [7] K. A. Takeuchi and M. Sano, *Phys. Rev. Lett.* **104**, 230601 (2010).
- [8] K. A. Takeuchi, M. Sano, T. Sasamoto, and H. Spohn, *Sci. rep.* **1**, 34 (2011).
- [9] K. A. Takeuchi and M. Sano, *J. Stat. Phys.* **147**, 853 (2012).
- [10] M. A. C. Huergo, M. A. Pasquale, A. E. Bolzán, A. J. Arvia, and P. H. González, *Phys. Rev. E* **82**, 031903 (2010); M. A. C. Huergo, M. A. Pasquale, P. H. González, A. E. Bolzán, and A. J. Arvia, *Phys. Rev. E* **84**, 021917 (2011); *Phys. Rev. E* **85**, 011918 (2012).
- [11] P. J. Yunker, M. A. Lohr, T. Still, A. Borodin, D. J. Durian, and A. G. Yodh, *Phys. Rev. Lett.* **110**, 035501 (2013).
- [12] S. Atis, A. K. Dubey, D. Salin, L. Talon, P. Le Doussal, and K. J. Wiese, *Phys. Rev. Lett.* **114**, 234502 (2015).
- [13] See K. A. Takeuchi, *J. Stat. Mech.: Th. Exp.* **2014**, P01006 (2014) for a review on experiments.
- [14] Following exact results for the flat KPZ subclass [16–18], here we define χ_1 by multiplying $2^{-2/3}$ to the standard random variable of the GOE Tracy-Widom distribution.
- [15] K. Johansson, *Comm. Math. Phys.* **209**, 437 (2000).
- [16] M. Prähofer and H. Spohn, *Phys. Rev. Lett.* **84**, 4882 (2000).
- [17] T. Sasamoto, *J. Phys. A: Math. Gen.* **38**, L549 (2005).
- [18] P. L. Ferrari and H. Spohn, *J. Phys. A: Math. Gen.* **38**, L557 (2005).
- [19] T. Sasamoto and H. Spohn, *Phys. Rev. Lett.* **104**, 230602 (2010).
- [20] G. W. Anderson, A. Guionnet, and O. Zeitouni, *An Introduction to Random Matrices* (Cambridge University Press, 2010).
- [21] M. Prähofer and H. Spohn, *J. Stat. Phys.* **108**, 1071 (2002).
- [22] P. G. de Gennes and J. Prost, *The Physics of Liquid Crystals* (Oxford Science Publications, 1995).
- [23] F. Wyrowski and O. Bryngdahl, *J. Opt. Soc. Am. A* **5**, 1058 (1988).
- [24] In order to avoid DSM2 nucleation by laser light uncontrolled by the SLM, we shifted the image from the focal point of the SLM imaging lens by superimposing the phase difference equivalent to a convex lens at the SLM.
- [25] When we calculated the cumulants with the experimental data, we obtained the cumulants of the fluctuations at each x and averaged them, in order to reduce the effect of heterogeneity of the cell and the initial condition.
- [26] K. A. Takeuchi, *J. Stat. Mech.: Th. Exp.* **2012**, P05007 (2012).
- [27] S. G. Alves, T. J. Oliveira, and S. C. Ferreira, *J. Stat. Mech.: Th. Exp.* **2013**, P05007 (2013).
- [28] S. Prolhac, *Phys. Rev. Lett.* **116**, 090601 (2016).
- [29] J. Baik and Z. Liu, (2016), arXiv:1605.07102.
- [30] I. S. S. Carrasco, K. A. Takeuchi, S. C. Ferreira, and T. J. Oliveira, *New J. Phys.* **16**, 123057 (2014).
- [31] F. Bornemann, *Math. Comp.* **79**, 871 (2010).